Quantifying the spin mixing conductance of EuO/W heterostructures by spin Hall magnetoresistance experiments

Cite as: Appl. Phys. Lett. **118**, 192401 (2021); https://doi.org/10.1063/5.0049235 Submitted: 02 March 2021 • Accepted: 23 April 2021 • Published Online: 10 May 2021

🧓 Paul Rosenberger, 🗓 Matthias Opel, 厄 Stephan Geprägs, et al.







ARTICLES YOU MAY BE INTERESTED IN

Spin-orbit torques: Materials, physics, and devices
Applied Physics Letters 118, 120502 (2021); https://doi.org/10.1063/5.0039147

Materials, physics, and devices of spin-orbit torque effect
Applied Physics Letters 118, 180401 (2021); https://doi.org/10.1063/5.0054652

Spin Hall magnetoresistance in antiferromagnetic insulators

Journal of Applied Physics 127, 243902 (2020); https://doi.org/10.1063/5.0009529

☐ QBLOX



Shorten Setup Time
Auto-Calibration
More Qubits

Fully-integrated
Quantum Control Stacks
Ultrastable DC to 18.5 GHz
Synchronized <<1 ns
Ultralow noise



100s qubits

visit our website >



Quantifying the spin mixing conductance of EuO/W heterostructures by spin Hall magnetoresistance experiments

Cite as: Appl. Phys. Lett. **118**, 192401 (2021); doi: 10.1063/5.0049235 Submitted: 2 March 2021 · Accepted: 23 April 2021 · Published Online: 10 May 2021







Paul Rosenberger,^{1,2,a)} D Matthias Opel,³ D Stephan Geprägs,³ D Hans Huebl,^{3,4,5} D Rudolf Gross,^{3,4,5} D Martina Müller,⁶ D and Matthias Althammer^{3,4,a)}

AFFILIATIONS

- ¹Peter Grünberg Institut (PGI-6), Forschungszentrum Jülich GmbH, D-52428 Jülich, Germany
- ²Fakultät Physik, Technische Universität Dortmund, 44227 Dortmund, Germany
- ³Walther-Meißner-Institut, Bayerische Akademie der Wissenschaften, 85748 Garching, Germany
- ⁴Physik-Department, Technische Universität München, 85748 Garching, Germany
- ⁵Munich Center for Quantum Science and Technology (MCQST), 80799 München, Germany
- ⁶Department of Physics, University of Konstanz, D-78457 Konstanz, Germany

ABSTRACT

The spin Hall magnetoresistance (SMR) allows to investigate the magnetic textures of magnetically ordered insulators in heterostructures with normal metals by magnetotransport experiments. We here report the observation of the SMR in *in situ* prepared ferromagnetic EuO/W thin film bilayers with magnetically and chemically well-defined interfaces. We characterize the magnetoresistance effects utilizing angle-dependent and field-dependent magnetotransport measurements as a function of temperature. Applying the established SMR model, we derive and quantify the real and imaginary parts of the complex spin mixing interface conductance. We find that the imaginary part is by one order of magnitude larger than the real part. Both decrease with increasing temperature. This reduction is in agreement with thermal fluctuations in the ferromagnet.

Published under an exclusive license by AIP Publishing. https://doi.org/10.1063/5.0049235

The spin Hall magnetoresistance (SMR) opened up the opportunity to study magnetically ordered insulators (MOIs) in bilayer heterostructures with normal metals (NM) via simple magnetotransport experiments.¹⁻⁴ Until today, the SMR was successfully employed to probe the magnetic moment configuration in ferrimagnetic, antiferromagnetic, and complex (e.g., canted or chiral) magnetic phases. 1,3,5-13 Initially, the role of magnetic sublattices was not considered in the SMR theory framework. However, later studies revealed that the effect is sensitive to the spin texture at the interface, in particular to the arrangement of the individual magnetic sublattices. This enabled studies on spin-canting in ferri- and antiferromagnetic insulators. 6-10,12,13 Interestingly, the SMR in ferromagnetic insulators has rarely been investigated, and only recently results on EuS/Pt and EuO/Pt interfaces have been reported. 14,15 The effect critically depends on the quality of the MOI/NM interface¹⁶ and, in particular, on its transparency for the spin current, described via the complex spin mixing interface conductance $G_{\uparrow\downarrow} = G_r + iG_i$. Most importantly, both experiments and theory

suggest that in such ferromagnetic insulators G_i exceeds G_r , as interface compensation effects do not reduce G_i . This opens up a different regime for SMR experiments as well as for spin-transfer torque effects.

In this Letter, we focus on the metastable ferromagnetic semiconductor EuO with a Curie temperature of 69 K. We first present an x-ray photoelectron spectroscopy (XPS) study on both EuO/Pt and EuO/W heterostructures, which reveals very differently defined chemical interfaces. Based on our findings, we focus on the well-defined ferromagnetic EuO/W heterostructure in order to investigate their magnetoresistance (MR) as a function of temperature and applied magnetic field orientation. We identify two contributions to the MR in these samples: (i) SMR originating from the EuO/W interface and (ii) ordinary MR from the metallic W layer. By extracting the SMR parameters, we quantify the real and imaginary parts of the spin mixing interface conductance in the limit of $G_{\rm i} > G_{\rm r}$. This allows us to investigate the temperature dependence of $G_{\rm i}$ and $G_{\rm r}$ and find that in agreement with theory, it is dominated by spin fluctuations.

^{a)}Authors to whom correspondence should be addressed: p.rosenberger@fz-juelich.de and matthias.althammer@wmi.badw.de

Epitaxial and bulk-like EuO thin films with a thickness of about 40 nm are deposited on single crystalline, (001)-oriented yttriastabilized zirconia (YSZ) substrates using oxide molecular beam epitaxy. 18,19 We applied our preparation process reported in Ref. 20, using a deposition temperature of 400 °C. After confirming the film quality by in situ XPS, RHEED, and LEED, we subsequently in situ deposit 4 nm thin W strips with a width of 250 μ m through a shadow mask onto the EuO film via electron beam evaporation. For comparison, we fabricate a reference sample consisting of W-strips with the same thickness deposited directly on a YSZ substrate. To protect the uncovered EuO from oxidation, we deposit a 15 nm MgO capping layer on all samples via electron beam evaporation. To further confirm the EuO quality, we perform SQUID magnetometry measurements. In order to probe the interface quality of EuO/Pt and EuO/W heterostructures by means of in situ XPS using a Al K_{α} source, we fabricate a second set of samples with plane thin films of 0.3 nm Pt and 0.4 nm W, respectively, deposited without shadow mask onto EuO films. For magnetotransport measurements, we use a standard four-point dc measurement technique in a 3D-vector magnet cryostat with a variable temperature insert. For all transport measurements, we use a charge current bias of 10 µA and a current reversal method to eliminate any spurious thermal signals in our measurements.4

First, we study the stoichiometry of EuO at the EuO/Pt and EuO/W interfaces by *in situ* XPS of the Eu $3d_{5/2}$ core level. To investigate the EuO interface through the metallic Pt and W capping layer, we compare spectra taken before and after the metal deposition. In detail, we subtract a constant background and normalize each spectrum to the Eu²⁺ $3d_{5/2}$ peak height.

The Eu 3d_{5/2} core-level spectra for the two different trilayers are depicted in Fig. 1. For the uncovered EuO films (dashed lines), we find only spectral contributions of Eu²⁺, indicating stoichiometric and, thus, ferromagnetic EuO. ^{19,22–24} After the W or Pt deposition (solid lines), the spectra show an enhanced inelastic background at the high

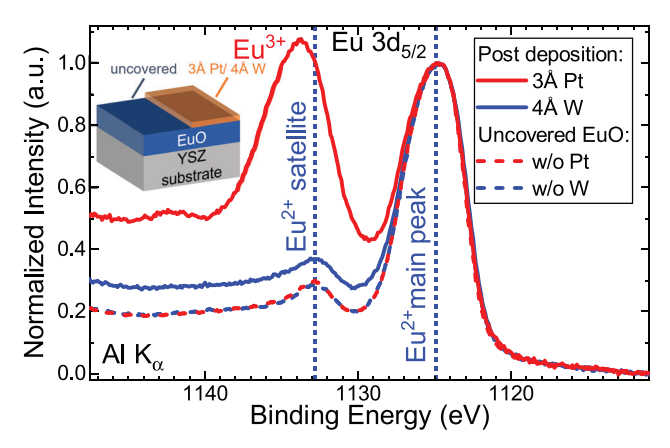


FIG. 1. Comparison of XPS results for *in situ* grown EuO/Pt and EuO/W bilayers. For the bare EuO films prior to Pt or W deposition (red and blue dashed lines), the Eu $3d_{5/2}$ core level exhibits the Eu²⁺ main peak and its satellite at the high binding energy side, indicating ferromagnetic EuO. After the deposition of 4 Å W, the inelastic background is slightly enhanced and only the pure Eu²⁺ observed (blue solid line). However, the deposition of 3 Å Pt results in an intense Eu³⁺ peak, indicating the overoxidation of the EuO/Pt interface toward paramagnetic Eu₂O₃ or Eu₃O₄ (red solid line).

binding energy side, which does not hamper the analysis of the EuO composition but simply originates from additional scattering of the photoelectrons while traversing the metal overlayer. For EuO/W, the spectrum in Fig. 1 also exhibits a pronounced Eu²⁺ main peak and a satellite at its higher binding energy side, i.e., the signature of pure Eu²⁺, indicating ferromagnetic EuO at the well-defined EuO/W interface.

For EuO/Pt, in contrast, we find an intense Eu³+ peak at an even higher binding energy compared to the Eu²+ satellite.²⁴ This observation of significant Eu oxidation may be explained by the catalytic property of Pt, which lowers the formation energy of Eu₂O₃ or Eu₃O₄. Our observation shows that the deposition of Pt onto a stoichiometric EuO film results in an interfacial oxidation process of the initially ferromagnetic EuO, which causes the formation of paramagnetic Eu₂O₃ or Eu₃O₄ by oxygen diffusion from the substrate and EuO layer to the interface.¹¹¹8 Thus, no sharp interface between a magnetically ordered insulator and a normal metal persists for this heterostructure. Hence, we focus on EuO/W heterostructures in the following.

For the investigation of the transport properties, we first perform angle-dependent magnetoresistance (ADMR) measurements. The orientation of an external magnetic field ${\bf h}$ with the constant magnitude $\mu_0 H$ is varied in three distinct rotation planes, while the longitudinal resistivity $\rho_{\rm long}$ of the sample is determined as a function of the rotation angle. The current direction ${\bf j}$ and the surface normal ${\bf n}$ define our orthogonal coordinate system via the transverse direction ${\bf t}={\bf n}\times{\bf j}$ (see illustration in Fig. 2). Utilizing these three-unit vectors, we define three orthogonal rotation planes for the magnetic field (referred to as ip, oopj, and oopt, see Fig. 2). Using all three rotation planes, we analyze the symmetry of the observed magnetoresistance to determine its origin. We calculate the longitudinal magnetoresistance $MR(\phi) = [\rho_{\rm long}(\phi)/\rho_{\rm long}(\phi=90^\circ)] - 1$ for $\phi=\alpha,\beta,\gamma$. In Fig. 2, we

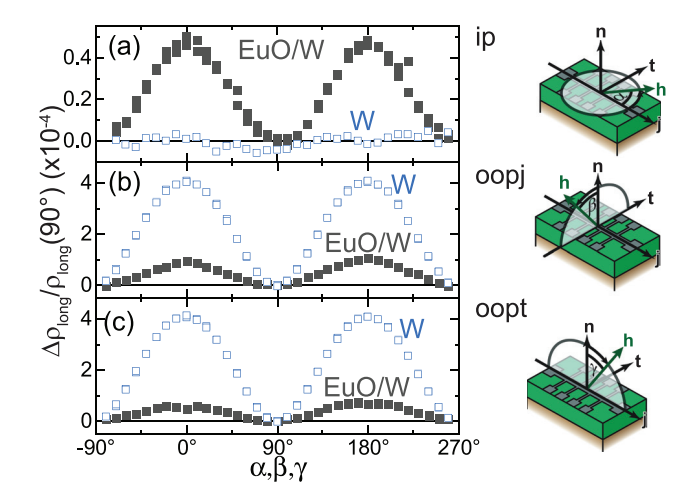


FIG. 2. Angle-dependent magnetotransport at $T=15\,\mathrm{K}$ and $\mu_0H=2\,\mathrm{T}$ for a EuO/W heterostructure (black squares) and a bare W film (open blue squares) utilizing (a) in-plane (ip) rotation plane, (b) out-of-plane perpendicular to \mathbf{j} (oopj) rotation plane, and (c) out-of-plane perpendicular to \mathbf{t} (oopt) rotation plane. The illustrations on the right show rotation plane of the external magnetic field with respect to the sample and current direction. For EuO/W, we observe in all rotation planes an angle-dependence of ρ_{long} , consistent with the combined action of SMR and ordinary MR. For the bare W layer, there is no angle-dependence visible in the ip rotation confirming that the EuO/W interface is necessary to observe the SMR signature.

show the obtained results for the bare W reference (blue open squares) and the EuO/W sample (black filled squares) at $T=15\,\mathrm{K}$ and $\mu_0H=2\,\mathrm{T}$.

For the bare W reference sample, we only observe an angle-dependence for the oopj and oopt rotations with a \cos^2 -dependence and a maximum $MR = 4 \times 10^{-4}$ for $\mathbf{h} \parallel \mathbf{n}$. Such a behavior is typical for an ordinary magnetoresistance (OMR), where the resistance of the sample increases if the magnetic field is applied perpendicular to the sample plane. In our samples, this OMR exhibits a quadratic magnetic field dependence [see Fig. 3(a)]. For the ip rotation plane, we do not find any systematic angle-dependence within the resolution ($MR < 5 \times 10^{-6}$) of our setup [Fig. 2(a)].

For our EuO/W sample, in contrast, we observe an angle-dependence for the ip rotation, following a \cos^2 behavior and showing a maximum of $MR = 5 \times 10^{-5}$ at $\mathbf{h} \parallel \mathbf{j}$. This angle-dependence and position of the maximum (i.e., its phase) are consistent with the SMR for ip rotations in ferrimagnetic insulators, where the magnetization follows the external magnetic field. In the case of the oopj rotation, the MR exhibits a \cos^2 dependence and maximum of $MR = 11 \times 10^{-5}$ for $\mathbf{h} \parallel \mathbf{n}$. For this rotation plane, both SMR and OMR of the W layer contribute to the MR. In the oopt rotation plane, where only the OMR contributes, we observe a \cos^2 angle-dependence and a maximum of $MR = 7 \times 10^{-5}$. The fact that the sum of the maximum MR for ip and oopt rotation planes nicely matches the maximum MR in the oopj rotation and confirms our assumption that two effects contribute to the MR in the EuO/W sample: the SMR of the EuO/W interface and the OMR of the W layer.

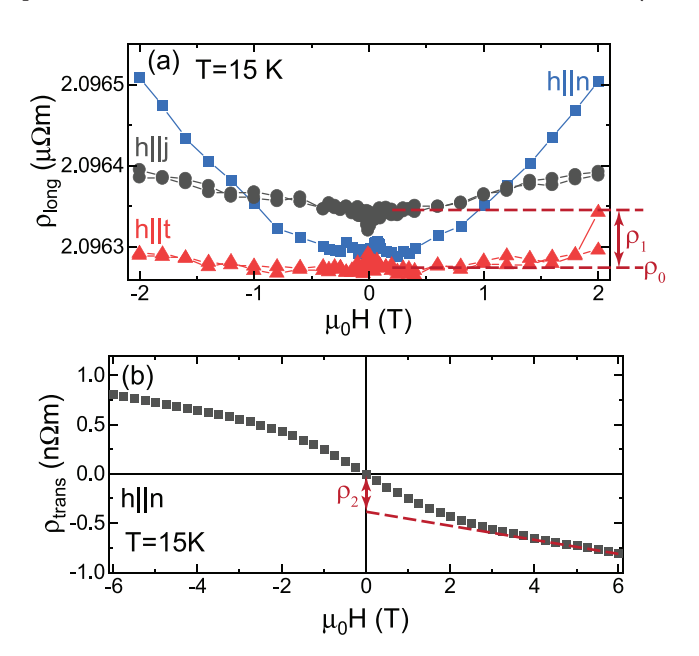


FIG. 3. Field-dependent magnetotransport for the EuO/W sample at $T=15\,\mathrm{K}$: (a) ρ_{long} as a function of the applied magnetic field for \mathbf{h} oriented along \mathbf{j} (black dots), \mathbf{t} (red triangles), and \mathbf{n} (blue squares). For $\mathbf{h} \parallel \mathbf{n}$, we observe a quadratic field dependence, typical for the OMR in W. (b) ρ_{trans} (black symbols) as a function of the applied magnetic field for $\mathbf{h} \parallel \mathbf{n}$. At large magnetic fields, a linear field dependence (dashed red line) originating from the ordinary Hall effect is observed. The red dashed lines and arrows in both panels illustrate the extraction of ρ_0 , ρ_1 , and ρ_2 from these measurements.

Moreover, since we do not observe any significant angle-dependence for the ip rotation in the W reference sample, we conclude that the EuO/W interface is crucial to observe the SMR effect. The SMR symmetry is attributed to spin current transfer across the EuO/W interface governed by the spin mixing conductance. We note that the OMR observed in the EuO/W bilayer is reduced by a factor of 6 as compared to the bare W reference sample. One may attribute this to the difference in the interface properties of the W layer on EuO and YSZ and the role of interface scattering for the OMR.

To complement the picture of the angle-dependent MR in our EuO/W sample, we also investigate the evolution of $\rho_{\rm long}$ as a function of the magnitude of the applied magnetic field $\mu_0 H$ for three fixed field orientations: $\mathbf{h} \parallel \mathbf{j}$, $\mathbf{h} \parallel \mathbf{t}$, and $\mathbf{h} \parallel \mathbf{n}$ (see illustration in Fig. 2 for a definition of these orientations). The results are plotted in Fig. 3(a) for T=15 K. Obviously, $\rho_{\rm long}$ is larger for ${\bf h}\parallel {\bf j}$ than for ${\bf h}\parallel {\bf t}$, which is fully consistent with the SMR nature of the in-plane MR. ¹⁻³ For these two field orientations, moreover, $\rho_{\rm long}$ increases gradually with increasing magnetic field magnitude. This weak magnetic field-dependence may either originate from a small Hanle MR^{25,26} only present in our EuO/W bilayer and not in the W reference sample, or a slight misalignment of the magnetic field with respect to the sample plane, such that the OMR sensitive to the out-of-plane magnetic field component also contributes in our measurements. As discussed in the supplementary material, we estimate an upper limit for the Hanle MR contribution of $0.8 \times 10^{-5} \,\mathrm{T}^{-1}$ for the EuO/W bilayer. For $\mathbf{h} \parallel \mathbf{n}$, ρ_{long} exhibits a pronounced, parabola-shaped magnetic field-dependence, as expected for an OMR in the W layer.

To complete the picture, we plot the magnetic field-dependence of the transverse resistivity $\rho_{\rm trans}$ for $\mathbf{h} \parallel \mathbf{n}$ in Fig. 3(b) at 15 K for the EuO/W sample. For large external magnetic fields, we observe a linear increase with negative slope in $\rho_{\rm trans}$ originating from the ordinary Hall effect in the W layer [dashed red line in Fig. 3(b)]. For small magnetic fields, $\mu_0 H \leq 3$ T, $\rho_{\rm trans}$ deviates from this linear dependence. We attribute this deviation to the SMR, which causes an anomalous Hall-like contribution to $\rho_{\rm trans}$. At these small fields, the magnetization of the EuO layer is no longer saturated along \mathbf{n} , but starts to align in the sample plane due to the increasing influence of shape anisotropy.

We carried out field-dependent MR experiments as a function of temperature (not shown here) for all three field orientations to further investigate the temperature-dependence of the SMR in our EuO/W sample. To quantify the SMR from these measurements, we utilize the SMR expression for $\rho_{\rm long}$ from Ref. 2

$$\rho_{\text{long}} = \rho_0 + \rho_1 (1 - m_t^2), \tag{1}$$

with $m_{\rm t}$ the projection of the magnetization orientation ${\bf m}$ in EuO onto the ${\bf t}$ -direction. From the field-dependent MR measurements for ${\bf h} \parallel {\bf j}$ ($m_{\rm t}=0$) and ${\bf h} \parallel {\bf t}$ ($m_{\rm t}=1$), we extract ρ_0 and ρ_1 as illustrated in Fig. 3(a) for $\mu_0 H=250$ mT, where the magnetization in the EuO is already saturated within the sample plane, and the influence of the magnetic field-dependence of $\rho_{\rm long}$ is negligible. For $\rho_{\rm trans}$, we write

$$\rho_{\text{trans}} = \rho_2 m_{\text{n}} + R_{\text{H}} \mu_0 H_{\text{n}} + \rho_3 m_{\text{j}} m_{\text{t}}, \qquad (2)$$

in the framework of the SMR theory² with m_n and m_t the projections of **m** onto **n** and **j**, respectively. In addition, R_H is the ordinary Hall constant and $\mu_0 H_n$ is the projection of the applied external magnetic

field onto **n**. For **h** \parallel **n** $(m_j, m_t = 0)$, we extract ρ_2 by linear fitting the ρ_{trans} data for $|\mu_0 H| > 4\,\mathrm{T}$ and extrapolating to zero magnetic field as indicated in Fig. 3(b). From the linear fit, we also extract $R_H \approx -8 \times 10^{-11}\,\Omega\,\mathrm{mT}^{-1}$ for our EuO/W bilayer in agreement with Hall measurements on W in previous studies. ²⁸

The results for ρ_1/ρ_0 and ρ_2/ρ_0 are plotted as a function of temperature in Fig. 4(a). For both SMR contributions, we observe an increase with decreasing T. The values for ρ_1/ρ_0 seem to saturate at low temperatures. Interestingly, both contributions vanish at 75 K, just above the Curie temperature $T_c \approx 69 \,\mathrm{K}$ determined from SQUID magnetometry measurements [see Fig. 4(b)], indicated by the grayshaded area in Figs. 4(a) and 4(b). Within our experimental resolution, we do not find any evidence that the SMR persists above T_c , as, for example, observed in Cr₂O₃/Pt bilayers.²⁹ As discussed further below, this may originate from the significant reduction of G_r and G_i due to the localized 4f-electrons contributing to the SMR for Eu²⁺ as opposed to the 3d-electrons in Cr3+. For all investigated temperatures, the absolute value of ρ_2/ρ_0 is larger than ρ_1/ρ_0 , which we attribute to the facts that $G_{\rm i} > G_{\rm r}$ for all temperatures (as quantified below) and ρ_2/ρ_0 is dominated by $G_{\rm i}$, whereas ρ_1/ρ_0 is dominated by $G_{\rm r}$. This finding is exactly opposite to the results obtained in ferrimagnetic yttrium iron garnet (YIG)/Pt heterostructures with in situ interfaces, where ρ_1/ρ_0 is always much larger than ρ_2/ρ_0 , and compensation effects significantly reduce G_i . 3,17,30

We now use the extracted temperature-dependent ρ_1/ρ_0 and ρ_2/ρ to extract values for the complex spin mixing conductance

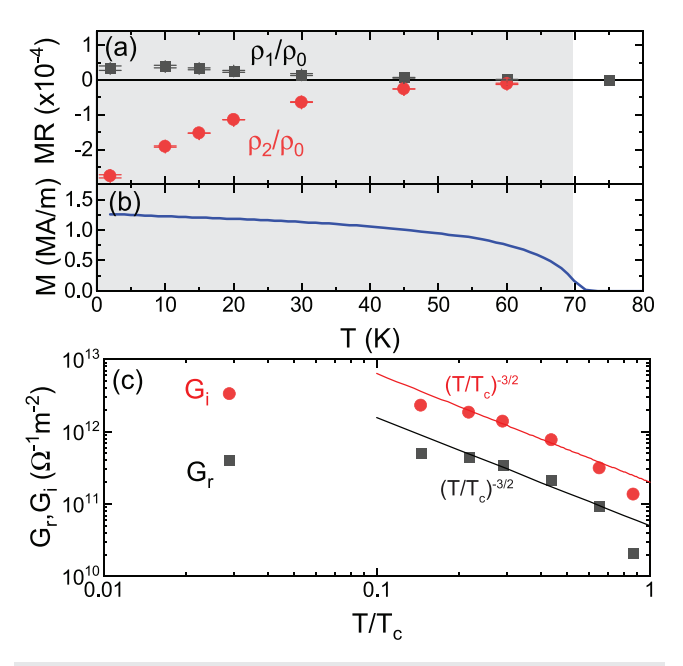


FIG. 4. (a) Temperature dependence of ρ_1/ρ_0 and ρ_2/ρ_0 extracted from the field-dependent magnetoresistance measurements on the EuO/W sample. (b) Magnetization vs temperature determined from SQUID magnetometry after field cooling the sample and measuring at zero magnetic field. (c) Extracted values for G_r (black squares) and G_i (red circles) as a function of the reduced temperature T/T_c . The black and red line indicate a $(T/T_c)^{-3/2}$ -dependence, which agrees well with the extracted temperature dependence for G_r and G_i in the intermediate T/T_c -range.

 $G_{\uparrow\downarrow} = G_{\rm r} + iG_{\rm i}$ of the EuO/W interface. From SMR theory,² we get the following expression for ρ_1/ρ_0 :

$$\frac{\rho_{1}}{\rho_{0}} = \frac{\theta_{\text{SH}}^{2}}{t_{\text{NM}}} \lambda_{\text{sf}} \operatorname{Re} \left[\frac{2\rho_{\text{NM}} \lambda_{\text{sf}} G_{\uparrow\downarrow} \tanh^{2} \left(\frac{t_{\text{NM}}}{2\lambda_{\text{sf}}} \right)}{1 + 2\rho_{\text{NM}} \lambda_{\text{sf}} G_{\uparrow\downarrow} \coth \left(\frac{t_{\text{NM}}}{\lambda_{\text{sf}}} \right)} \right], \tag{3}$$

with $\theta_{\rm SH}$ the spin Hall angle, $\lambda_{\rm sf}$ the spin diffusion length, $\rho_{\rm NM}$ the resistivity, and $t_{\rm NM}$ the thickness of the NM. For ρ_2/ρ_0 , we write down the following expression from SMR theory:

$$\frac{\rho_{2}}{\rho_{0}} = -\frac{\theta_{\rm SH}^{2}}{t_{\rm NM}} \lambda_{\rm sf} \operatorname{Im} \left[\frac{2\rho_{\rm NM} \lambda_{\rm sf} G_{\uparrow\downarrow} \tanh^{2} \left(\frac{t_{\rm NM}}{2\lambda_{\rm sf}}\right)}{1 + 2\rho_{\rm NM} \lambda_{\rm sf} G_{\uparrow\downarrow} \coth \left(\frac{t_{\rm NM}}{\lambda_{\rm sf}}\right)} \right]. \tag{4}$$

It is important to note that in most previous reports, the above expressions were approximated for the case of $G_r \gg G_i$, a valid assumption for ferrimagnetic and antiferromagnetic insulators, where compensation effects can drastically reduce G_i . For ferromagnetic insulators, we need to account for G_r and G_i , which especially leads to contributions of G_i to ρ_1/ρ_0 , mostly neglected for ferriand antiferromagnetic insulators. Assuming $\lambda_{\rm sf}\rho_{\rm NM}G_r\ll 1$ (spin transparency of the interface far away from the ideal limit), we obtain the following approximation for G_i by combining Eqs. (3) and (4):

$$G_{\rm i} \approx \frac{\rho_{2}\rho_{0}^{-1} - \left[\rho_{1}\rho_{0}^{-1}\rho_{2}\rho_{0}^{-1}\left[\theta_{\rm SH}^{2}t_{\rm NM}^{-1}\lambda_{\rm sf}^{2}\rho_{0}\tanh\left(\frac{t_{\rm NM}}{2\lambda_{\rm sf}}\right)\right]^{-1}\right]}{-\theta_{\rm SH}^{2}t_{\rm NM}^{-1}\lambda_{\rm sf}^{2}\rho_{0}\tanh\left(\frac{t_{\rm NM}}{2\lambda_{\rm sf}}\right)}.$$
 (5)

Within this approximation, we have set $\rho_{\rm NM}=\rho_0$, as ρ_0 is determined from the field-dependent MR measurements. Gr can then be determined from Eq. (3) and inserting the approximated G_i . We obtain a quadratic equation for G_r , such that two solutions for G_r exist. We select the solution with the correct temperature dependence of the absolute value of G_r (decreasing with increasing temperature). To quantify G_r and G_i, we assume temperature-independent $\lambda_{sf}=1.5\,\mathrm{nm}$ and $\theta_{SH}=0.2$ for W taking into account the mixed phase of α - and β -W in our sample. Not accounting for a temperature dependence of these two parameters is justified by the weak temperature dependence of ρ of the W layer, as θ_{SH} and λ_{sf} depend on the NM resistivity. 32,33 For our EuO/W sample, ρ only changes by 1.4×10^{-2} in the investigated temperature range. We want to emphasize that a change of the assumed values for $\lambda_{\rm sf}$ and $\theta_{\rm SH}$ will only influence the absolute numbers of G_r and G_i , but does not affect the general temperature dependence for the two parameters. The results of this procedure are shown in Fig. 4(c) as a function of the reduced temperature T/T_c .

For low temperatures, we find $G_r = 4 \times 10^{11} \,\Omega^{-1} \,\mathrm{m}^{-2}$ and $G_i = 3 \times 10^{12} \,\Omega^{-1} \,\mathrm{m}^{-2}$. The obtained values agree well with results on EuS/Pt. Compared to YIG/Pt interfaces, 3,30,34 however, the extracted G_r is significantly reduced for the EuO/W interface, indicating a lower coupling strength between the mobile electrons in the NM and the localized electrons of the magnetic moments in EuO. We attribute this observation to the different orbital nature of the localized

electrons. For ${\rm Eu}^{2+}$, the localized electrons are in 4f-orbitals, while for ${\rm Fe}^{3+}$, they are located in 3d-orbitals. Thus, we assume that coupling effects via orbital overlap are reduced for EuO as compared to YIG, which reasonably explains the differences between YIG/NM and EuO/NM interfaces.

For $G_{\rm r}$ and $G_{\rm i}$, we observe a monotonous decrease with increasing temperature. The temperature-dependence of $G_{\rm r}$ and $G_{\rm i}$ is explained by the influence of thermal fluctuations in the magnetic lattice of the MOI.^{17,35,36} In this way, we can describe the temperature dependence as $G_{\rm r} \approx (1-2n/s)G_{\rm r}(T=0)$ and $G_{\rm i} \approx (1-n/s)G_{\rm i}(T=0)$, where n is the density of magnons per unit cell and s is the saturation magnetization per unit cell in units of ${\rm h}$. In the limit of a three dimensional ferromagnet with parabolic magnon band dispersion and an intermediate $T/T_{\rm c}$ -range, both $G_{\rm r}$ and $G_{\rm i}$ should follow a $(T/T_{\rm c})^{-3/2}$ law, i.e., they scale inversely as the number of magnons. Indeed for $0.1 < T/T_{\rm c} < 0.7$, the extracted $G_{\rm r}$ and $G_{\rm i}$ agree well with a $(T/T_{\rm c})^{-3/2}$ dependence [black and red line in Fig. 4(c)], further confirming the theoretical model.

In summary, we present a detailed study of the MR in EuO/W bilayers. Initial XPS studies on both EuO/Pt and EuO/W heterostructures revealed a well-defined interface only for the EuO/W system. In this sample, we find two contributions to the observed MR: SMR and ordinary MR. We utilize the SMR contribution and its temperature dependence to quantify $G_{\rm r}$ and $G_{\rm i}$. From this analysis, we find $G_{\rm i} > G_{\rm r}$ for our EuO/W sample consistent with recent experiments on EuS/Pt interfaces. Our results confirm that in ferromagnetic insulators, a different regime for spin-transfer torque experiments can be established, where the field-like symmetry is the dominant contribution. Moreover, our approach to quantify $G_{\rm r}$ and $G_{\rm i}$ provides an alternative approach to investigate the spin mixing conductance, if the spin transport parameters $\theta_{\rm SH}$ and $\lambda_{\rm sf}$ and their temperature dependence of the NM are well known.

See the supplementary material for magnetic hysteresis loops of the EuO/W bilayer from SQUID magnetometry and a discussion of the magnetic field dependence of the magnetoresistance in the Eu/W bilayer and W reference sample.

We acknowledge the financial support by the German Research Foundation (Deutsche Forschungsgemeinschaft, DFG) via Germany's Excellence Strategy—No. EXC-2111–390814868 and Project No. AL 2110/2-1. P.R. and M.M. acknowledged the financial support by the International Collaborative Research Center No. TRR160 (Project C9).

DATA AVAILABILITY

The data that support the findings of this study are available from the corresponding author upon reasonable request.

REFERENCES

- ¹H. Nakayama, M. Althammer, Y.-T. Chen, K. Uchida, Y. Kajiwara, D. Kikuchi, T. Ohtani, S. Geprägs, M. Opel, S. Takahashi, R. Gross, G. E. W. Bauer, S. T. B. Goennenwein, and E. Saitoh, Phys. Rev. Lett. 110, 206601 (2013).
- ²Y.-T. Chen, S. Takahashi, H. Nakayama, M. Althammer, S. T. B. Goennenwein, E. Saitoh, and G. E. W. Bauer, Phys. Rev. B 87, 144411 (2013).
- ³M. Althammer, S. Meyer, H. Nakayama, M. Schreier, S. Altmannshofer, M. Weiler, H. Huebl, S. Geprägs, M. Opel, R. Gross, D. Meier, C. Klewe, T. Kuschel, J.-M. Schmalhorst, G. Reiss, L. Shen, A. Gupta, Y.-T. Chen, G. E. W. Bauer, E. Saitoh, and S. T. B. Goennenwein, Phys. Rev. B 87, 224401 (2013).

- ⁴M. Althammer, J. Phys. D **51**, 313001 (2018).
- ⁵A. Aqeel, N. Vlietstra, J. A. Heuver, G. E. W. Bauer, B. Noheda, B. J. van Wees, and T. T. M. Palstra, Phys. Rev. B 92, 224410 (2015).
- ⁶K. Ganzhorn, J. Barker, R. Schlitz, B. A. Piot, K. Ollefs, F. Guillou, F. Wilhelm, A. Rogalev, M. Opel, M. Althammer, S. Geprägs, H. Huebl, R. Gross, G. E. W. Bauer, and S. T. B. Goennenwein, Phys. Rev. B **94**, 094401 (2016).
- ⁷Y. Ji, J. Miao, K. K. Meng, Z. Y. Ren, B. W. Dong, X. G. Xu, Y. Wu, and Y. Jiang, Appl. Phys. Lett. **110**, 262401 (2017).
- ⁸G. R. Hoogeboom, A. Aqeel, T. Kuschel, T. T. M. Palstra, and B. J. van Wees, Appl. Phys. Lett. 111, 052409 (2017).
- ⁹J. Fischer, O. Gomonay, R. Schlitz, K. Ganzhorn, N. Vlietstra, M. Althammer, H. Huebl, M. Opel, R. Gross, S. T. B. Goennenwein, and S. Geprägs, Phys. Rev. B 97, 014417 (2018).
- ¹⁰L. Baldrati, A. Ross, T. Niizeki, C. Schneider, R. Ramos, J. Cramer, O. Gomonay, M. Filianina, T. Savchenko, D. Heinze, A. Kleibert, E. Saitoh, J. Sinova, and M. Kläui, Phys. Rev. B 98, 024422 (2018).
- ¹¹J. Fontcuberta, H. B. Vasili, J. Gàzquez, and F. Casanova, Adv. Mater. Interfaces 6, 1900475 (2019).
- ¹²J. Fischer, M. Althammer, N. Vlietstra, H. Huebl, S. T. Goennenwein, R. Gross, S. Geprägs, and M. Opel, Phys. Rev. Appl. 13, 014019 (2020).
- ¹³S. Geprägs, M. Opel, J. Fischer, O. Gomonay, P. Schwenke, M. Althammer, H. Huebl, and R. Gross, J. Appl. Phys. 127, 243902 (2020).
- ¹⁴J. M. Gomez-Perez, X.-P. Zhang, F. Calavalle, M. Ilyn, C. González-Orellana, M. Gobbi, C. Rogero, A. Chuvilin, V. N. Golovach, L. E. Hueso, F. S. Bergeret, and F. Casanova, Nano Lett. 20, 6815 (2020).
- ¹⁵K. Mallick, A. A. Wagh, A. Ionescu, C. H. W. Barnes, and P. S. Anil Kumar, Appl. Phys. Lett. **116**, 202405 (2020).
- ¹⁶S. Geprägs, C. Klewe, S. Meyer, D. Graulich, F. Schade, M. Schneider, S. Francoual, S. P. Collins, K. Ollefs, F. Wilhelm, A. Rogalev, Y. Joly, S. T. B. Goennenwein, M. Opel, T. Kuschel, and R. Gross, Phys. Rev. B 102, 214438 (2020).
- ¹⁷X.-P. Zhang, F. S. Bergeret, and V. N. Golovach, Nano Lett. **19**, 6330 (2019).
- ¹⁸T. Gerber, P. Lömker, B. Zijlstra, C. Besson, D. N. Mueller, W. Zander, J. Schubert, M. Gorgoi, and M. Müller, J. Mater. Chem. C 4, 1813 (2016).
- ¹⁹P. Lömker and M. Müller, Phys. Rev. Mater. **3**, 061401 (2019).
- G. M. Prinz, T. Gerber, A. Lorke, and M. Müller, Appl. Phys. Lett. 109, 202401 (2016).
 M. Schreier, N. Roschewsky, E. Dobler, S. Meyer, H. Huebl, R. Gross, and S. T. B. Goennenwein, Appl. Phys. Lett. 103, 242404 (2013).
- ²²P. Lömker, T. C. Rödel, T. Gerber, F. Fortuna, E. Frantzeskakis, P. L. Fèvre, F. Bertran, M. Müller, and A. F. Santander-Syro, Phys. Rev. Mater. 1, 062001 (2017)
- ²³M. Müller, G.-X. Miao, and J. S. Moodera, J. Appl. Phys. **105**, 07C917 (2009).
- ²⁴C. Caspers, M. Müller, A. X. Gray, A. M. Kaiser, A. Gloskovskii, C. S. Fadley, W. Drube, and C. M. Schneider, Phys. Rev. B 84, 205217 (2011).
- ²⁵S. Vélez, V. N. Golovach, A. Bedoya-Pinto, M. Isasa, E. Sagasta, M. Abadia, C. Rogero, L. E. Hueso, F. S. Bergeret, and F. Casanova, Phys. Rev. Lett. 116, 016603 (2016).
- ²⁶M. I. Dyakonov, Phys. Rev. Lett. **99**, 126601 (2007).
- ²⁷S. Meyer, R. Schlitz, S. Geprägs, M. Opel, H. Huebl, R. Gross, and S. T. B. Goennenwein, Appl. Phys. Lett. 106, 132402 (2015).
- ²⁸Q. Hao, W. Chen, and G. Xiao, Appl. Phys. Lett. **106**, 182403 (2015).
- ²⁹R. Schlitz, T. Kosub, A. Thomas, S. Fabretti, K. Nielsch, D. Makarov, and S. T. B. Goennenwein, Appl. Phys. Lett. 112, 132401 (2018).
- ³⁰S. Meyer, M. Althammer, S. Geprägs, M. Opel, R. Gross, and S. T. B. Goennenwein, Appl. Phys. Lett. **104**, 242411 (2014).
- ⁵¹C.-F. Pai, L. Liu, Y. Li, H. W. Tseng, D. C. Ralph, and R. A. Buhrman, Appl. Phys. Lett. **101**, 122404 (2012).
- ³²E. Sagasta, Y. Omori, M. Isasa, M. Gradhand, L. E. Hueso, Y. Niimi, Y. Otani, and F. Casanova, Phys. Rev. B 94, 060412 (2016).
- ³³E. Sagasta, Y. Omori, S. Vélez, R. Llopis, C. Tollan, A. Chuvilin, L. E. Hueso, M. Gradhand, Y. Otani, and F. Casanova, Phys. Rev. B 98, 060410 (2018).
- ³⁴M. Weiler, M. Althammer, M. Schreier, J. Lotze, M. Pernpeintner, S. Meyer, H. Huebl, R. Gross, A. Kamra, J. Xiao, Y.-T. Chen, H. Jiao, G. E. W. Bauer, and S. T. B. Goennenwein, Phys. Rev. Lett. 111, 176601 (2013).
- 35S. A. Bender and Y. Tserkovnyak, Phys. Rev. B 91, 140402 (2015).
- ³⁶X. G. Wang, Z. W. Zhou, Y. Z. Nie, Q. L. Xia, and G. H. Guo, Phys. Rev. B 97, 094401 (2018).